ACS OMEGA

http://pubs.acs.org/journal/acsodf
Article

Au-Decorated Ti_3C_2 MXene Sensor for Enhanced Detection of Gaseous Toxins (CO, $COCl_2$, H_2S, NH_3, NO_2): A DFT Study

Muhammad Huzaifa, Muhammad Shafiq, Nida Ali, Caterina Cocchi, Mohammad Nur-e-Alam, and Zaheer Ul-Haq*

Cite This: *ACS Omega* 2025, 10, 1562−1570
Read Online
ACCESS | Metrics & More | Article Recommendations

ABSTRACT: The rising level of toxic gases in the environment poses a high demand for efficient gas sensing materials. MXenes, an emerging class of two-dimensional (2D) materials, have gained significant interest in this area for having an active-site rich structure, tunable surface properties, and remarkable stability. Herein, an extensive density functional theory (DFT) study is conducted to investigate the sensing properties of pristine and Au-functionalized Ti_3C_2 MXene for five toxic gas molecules: CO, $COCl_2$, H_2S, NH_3, and NO_2. Pristine Ti_3C_2 displays high affinity for CO, H_2S, and NH_3, as assessed by density of states and a large binding energy, resulting in the chemisorption of these gas molecules providing a relatively large recovery time. In contrast, Au-functionalized Ti_3C_2 is able to sense all five toxins which are physisorbed on it, as indicated by lower adsorption energy and faster recovery time. As an example, the adsorption energy computed for CO is −0.14 eV and the resulting recovery time 0.21 ns. These results reveal that Au-functionalized Ti_3C_2 can serve as a highly efficient material for toxic gas sensing, particularly CO.

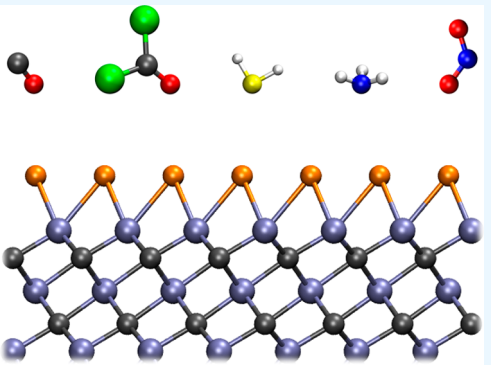

1. INTRODUCTION

Chemical gas sensors are extensively used in many industries, such as automotive, medical, process automation, safety, product and quality control, as well as pollution monitoring.[1] Due to the growing needs arising from environmental changes, scientists are searching for efficient sensing materials.[2] Two-dimensional (2D) materials are currently revolutionizing the gas-sensing industry.[3] In addition to being cost- and energy-efficient, they provide exceptional sensitivity to a wide range of gases.[4] Notably, 2D materials have a large surface-to-volume ratio, which equips them with an extended active surface area for gas-molecule interaction.[5] This property enhances their sensing ability enabling them to detect up to parts-per-billion (ppb) pollutant concentrations.[6] However, these materials have certain limitations as they require extremely lengthy recovery periods and have constraints on accuracy.[7]

Toxic and hazardous gases, including phosgene ($COCl_2$) and carbon monoxide (CO), are frequently utilized in manufacturing industries.[8] Incomplete combustion of fuels results in the formation of severely harmful carbon monoxide. This gas is challenging to detect for having colorless, tasteless, and odorless properties.[9] The primary sources of carbon monoxide emissions in the environment are industrial activities, automobile exhaust, and fossil fuel consumption.[10] By binding with hemoglobin in blood, carbon monoxide poses significant life threats.[11] Upon inhalation, it enters the body and reaches the bloodstream, displacing oxygen and causing the heart and brain to malfunction due to oxygen deprivation.[12] The most common signs of CO accumulation in the human body are fatigue and headache. Elevated CO levels cause brain damage, unconsciousness, and even death.[13] Phosgene, a toxic gas, is a key ingredient in making polyurethanes.[14] Despite being hazardous, it is also an important substrate in making isocyanates and insecticides.[15] Phosgene poses a significant threat to human life due to its subtle smell and delayed symptom onset, making it difficult to detect. Although it can be identified at 0.4 ppm, this is still above the safe exposure limit for humans.[16] Particularly, the toxicity of this gas arises from its destructive effect on the pulmonary alveoli proteins. By damaging the blood-air barrier, phosgene ultimately causes asphyxiation.[17] Due to high toxicity of these gases, various nanomaterials (graphene,[18,19] graphdiyne,[20] phosphorene,[21−23] MoS_2,[24] and many more[25−27]) for their sensing have been explored.

MXenes are a class of 2D materials composed of transition metal atoms and nonmetallic species like carbon or nitrogen as well as other elements including oxygen, sulfur, and chlorine,

Received: October 16, 2024
Revised: December 7, 2024
Accepted: December 16, 2024
Published: December 23, 2024

and characterized by high electrical conductivity, tunable surface chemistry, and excellent mechanical strength.[28] A detailed analysis of how MXenes interact with gas molecules has revealed the complex processes involved in their gas sensing activity.[29] This knowledge has led to the development of MXene-based highly sensitive gas detectors with great selectivity, which are relevant for several applications.[30] In particular, MXenes revolutionized gas sensors, making it possible to detect a broad spectrum of toxic gases, including nitrogen dioxide (NO_2),[31] ammonia (NH_3),[32] carbon monoxide (CO),[33,34] $COCl_2$,[35] and hydrogen sulfide (H_2S).[36] Due to the unique properties of MXenes, researchers across the globe are focusing on unlocking their critical gas sensing capabilities, minimizing experimental risks.[37,38]

Ab initio studies are widely used for their unparalleled atomic-level insights into sensing mechanisms and material properties.[39] Simulations have revealed that MXene surface terminations govern their interactions with gas molecules.[40] The synthesis of the titanium carbide ($Ti_3C_2T_x$) MXene opened a new frontier in materials research. Naguib et al.[38] established a comprehensive understanding of the unique two-dimensional material, achieved by integrating theoretical and experimental approaches. Extending this study, many researchers have directed their attention toward MXene-based material as gas sensors.[41−43] MXenes with hydroxyl groups strongly react with NO_2 due to a strong chemical interaction of NO_2 with these functionalities. In contrast, fluorine-terminated MXenes show high sensitivity for NH_3, resulting from the Lewis acid−base interaction between NH_3 and fluorine.[44] To enhance the response toward NH_3 or other gases, different techniques, such as doping[45] and noble metal decoration[46] have been proposed.

In the present study based on density functional theory (DFT), pristine and Au-functionalized Ti_3C_2 MXenes are investigated as platforms for sensing toxic gas molecules such as CO, $COCl_2$, H_2S, NH_3, and NO_2. The optimized structures, electronic properties, and adsorption performance against the sample gases are evaluated together with the sensing performance of the material in terms of the recovery time.

2. METHODOLOGY

All DFT calculations presented in this work were carried out with the CP2K code[47] applying periodic boundary conditions to account for the in-plane periodicity of the systems. Spin-polarization was considered due to the presence of transition metal atoms. Double-zeta valence with polarization (DZVP) molecularly optimized basis sets[48] and Goedecker−Teter−Hutter pseudopotentials[49] were used. The generalized gradient approximation (GGA) as implemented in the Perdew−Burke−Ernzerhof (PBE) exchange-correlation functional was adopted[50] including the Grimme-D3 scheme to account for van der Waals interactions between MXenes and gas molecules.[51] The plane-wave energy cutoff was set to 450 Ry and all the systems were relaxed below the force threshold of 0.01 eV/Å per atom. The Broyden−Fletcher−Goldfarb−Shanno (BFGS) algorithm was used for geometry optimization. Bader charges on gas molecules were computed with Critic2 code.[52] Furthermore, a vacuum space of 20 Å was added perpendicular to the MXene basal plane to avoid artificial interactions between neighboring images. All the studied systems were visualized with VMD software package.[53]

The adsorption energy (E_{ads}) of the gas molecule was calculated as

$$E_{ads} = E_{sys} - E_{MXene} - E_{gas} \quad (1)$$

where E_{sys} is the total energy of the gas@MXene system, E_{MXene} is the total energy of the Ti_3C_2/Au−Ti_3C_2 slab, and E_{gas} is the total energy of the isolated gas molecule.

The sensor recovery time (τ) was calculated as[54,55]

$$\tau = \nu_0^{-1} e^{-E_{ads}/kT} \quad (2)$$

where ν_0 is the attempt frequency, k is the Boltzmann constant, and T is the temperature. The values of attempt frequency and temperature were set to 10^{12} s^{-1} and 298 K, respectively.[24,56]

The work function (ϕ) of the studied systems was evaluated as[57]

$$\phi = E_{inf} - E_F \quad (3)$$

where E_{inf} is the electrostatic potential energy at infinity or vacuum and E_F is the Fermi energy.

3. RESULTS AND DISCUSSION

3.1. Structural and Adsorption Properties. The structure of the Ti_3C_2 MXene is characterized by 5 alternating layers of C and Ti atoms with the latter at the interface with vacuo. The Au-functionalization of this material is achieved by bonding a layer of gold to the outermost layers of Ti atoms, see Figure 1, where the 4 × 4 supercell adopted in the simulations of gas adsorption is depicted. While the hexagonal symmetry of the Ti_3C_2 unit cell remains unchanged after functionalization with gold atoms, the in-plane lattice constant of the unit cell of Ti_3C_2 is increased by 0.16% with Au-decoration and the resulting slab thickness of the surface-modified MXene is 1.92 times that of the pristine one, see Table 1. In addition, Au atoms at hexagonal sites show triple coordination with Ti atoms with a bond length of 2.77 Å. The Ti_1−C bond length

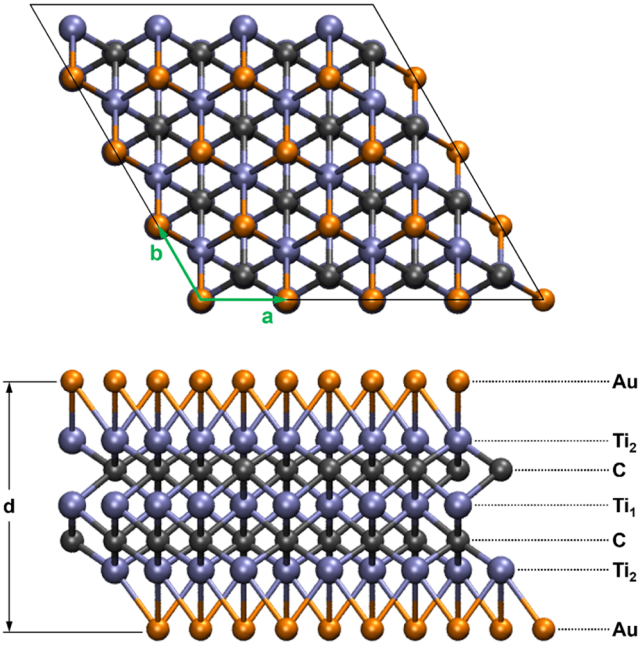

Figure 1. Top and side views of the optimized structure of the 4 × 4 supercell of the Au-decorated MXene, where the overall layer thickness d is indicated. Lattice parameters are shown with green arrows.

https://doi.org/10.1021/acsomega.4c09428
ACS Omega 2025, 10, 1562−1570

Table 1. Optimized Lattice Constant (a), Slab Thickness (d), and Bond Lengths of Pristine and Au-Decorated Ti_3C_2 MXene

			bond lengths (Å)		
system	a (Å)	d (Å)	Ti_1-C	Ti_2-C	Ti_2-Au
Ti_3C_2	3.07	4.63	2.20	2.03	
$Au-Ti_3C_2$	3.08	8.91	2.19	2.07	2.77

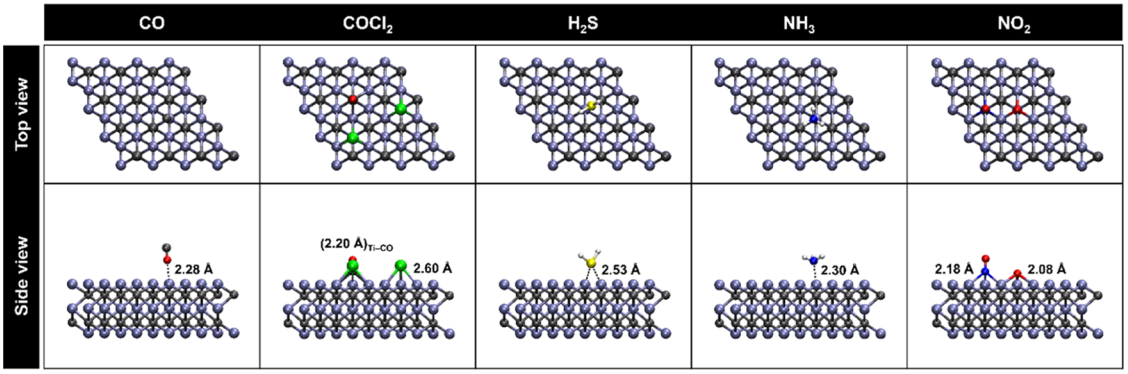

Figure 2. Optimized structures of the studied toxins at the pristine Ti_3C_2 surface.

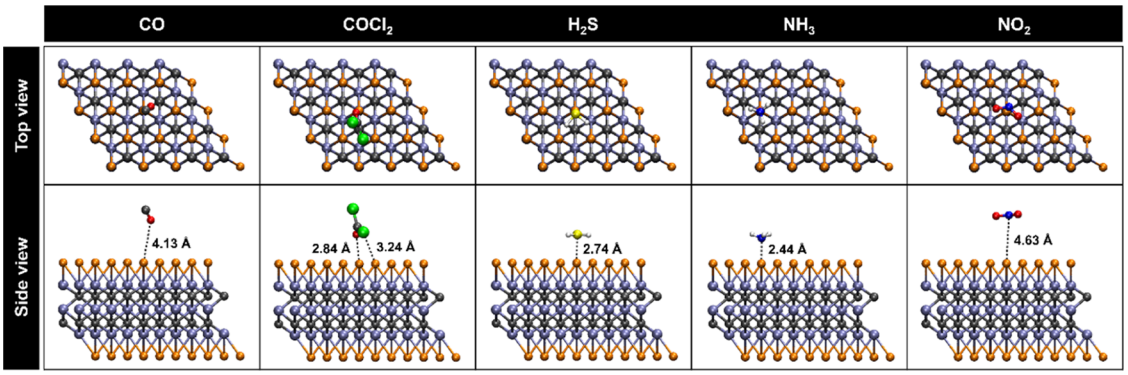

Figure 3. Optimized configurations of the studied toxins at the $Au-Ti_3C_2$ surface with the minimal distances from the substrates indicated by dotted lines in each plot.

Table 2. Adsorption Energies (E_{ads}) of the Studied Toxic Gases and the Sensor Recovery Time (τ) of Pristine and Au-Decorated Ti_3C_2

system	E_{ads} (eV)	τ (s)
$CO@Ti_3C_2$	−0.33	3.53×10^{-07}
$COCl_2@Ti_3C_2$		
$H_2S@Ti_3C_2$	−1.40	4.64×10^{11}
$NH_3@Ti_3C_2$	−1.19	1.29×10^{08}
$NO_2@Ti_3C_2$		
$CO@Au-Ti_3C_2$	−0.14	2.11×10^{-10}
$COCl_2@Au-Ti_3C_2$	−0.54	0.0016
$H_2S@Au-Ti_3C_2$	−0.71	1.07
$NH_3@Au-Ti_3C_2$	−0.66	0.13
$NO_2@Au-Ti_3C_2$	−0.68	0.32

Table 3. Performance Comparison of Various Gas Sensing Materials

material	gas	E_{ads} (eV)	τ (s)	references
$Au-Ti_3C_2$	CO	−0.14	2.11×10^{-10}	this study
In_2O_3		−0.52	6.17×10^{-04}	58
Co-g-GaN		−1.22	4.10×10^{08}	59
$Au-Ti_3C_2$	$COCl_2$	−0.54	0.0016	this study
Si-embedded MoS_2		−1.23	5.77×10^{08}	24
Al−Pc		−0.86	3.47×10^{02}	60
$Au-Ti_3C_2$	H_2S	−0.71	1.07	this study
In_2O_3		−2.35	5.30×10^{27}	58
Mn-doped BP		−0.85	2.70	61
$Au-Ti_3C_2$	NH_3	−0.66	0.13	this study
Rh-InSe		−1.11	5.64×10^{06}	62
Co-g-GaN		−0.68	0.30	59
$Au-Ti_3C_2$	NO_2	−0.68	0.32	this study
Rh-InSe		−3.09	1.52×10^{40}	62
Co-g-GaN		−3.67	1.00×10^{50}	59

decreases by 0.41% in Au-functionalized Ti_3C_2 whereas the Ti_2-C bond length is relaxed by 1.57%.

The adsorption of CO, $COCl_2$, H_2S, NH_3, and NO_2 is first simulated on the pristine Ti_3C_2 surface, see Figure 2. $COCl_2$ and NO_2 chemically react with the surface and are therefore not considered in the subsequent analysis. The CO molecule is bound to the surface Ti atom in a vertical configuration forming a Ti_2-O bond with length 2.28 Å; the corresponding adsorption energy is −0.33 eV. The adsorption of H_2S takes place through the coordination of the S atom with two adjacent Ti atoms at a distance of 2.53 Å from each of them and with an energy release of −1.40 eV. The optimized geometry of NH_3 adsorbed on Ti_3C_2 shows the molecule lying on top of the surface with the N atom facing Ti and forming a

https://doi.org/10.1021/acsomega.4c09428
ACS Omega 2025, 10, 1562−1570

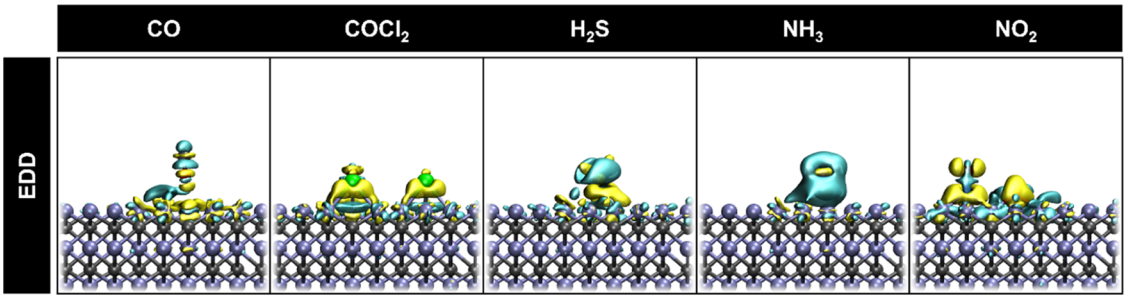

Figure 4. Electron density difference (EDD) between pristine Ti_3C_2 and the studied gases. Yellow (cyan) isosurfaces represent charge accumulation (depletion). Isovalues set to 0.0008 e/Å^3.

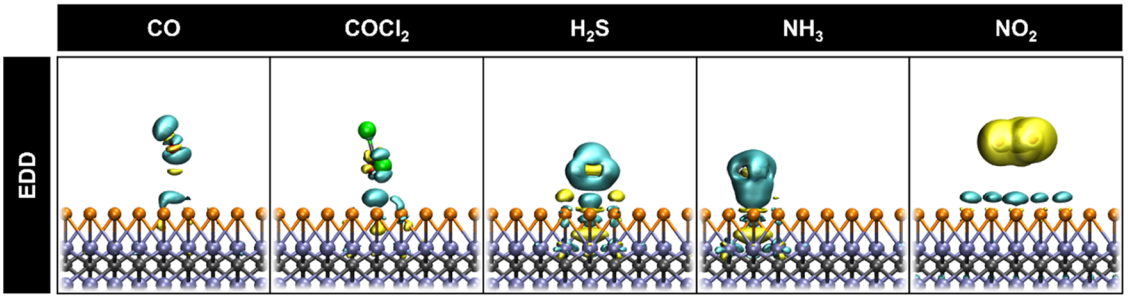

Figure 5. Electron density difference (EDD) between Au−Ti_3C_2 and the studied gas molecules. Yellow (cyan) isosurfaces represent charge accumulation (depletion). Isovalues set to 0.0008 e/Å^3.

Ti_2−N bond of length 2.30 Å with a binding energy of −1.19 eV.

Moving on to the study of gas adsorption on Au-functionalized Ti_3C_2 (see Figure 3), we find physisorption in all considered cases, with comparatively large bond distances and weak interactions between the adsorbents and the underlying Au atoms. A slightly tilted configuration of CO with respect to the surface normal appears with the O pointing to the closest Au atom at a distance of 4.13 Å: an adsorption energy of −0.14 eV is obtained in this case. Both values indicate a rather weak interaction between adsorbent and substrate. The adsorption of $COCl_2$ involves the formation of an Au−O bond with length 2.84 Å while the Au−Cl interaction is markedly ionic with the two atoms at a distance of 3.24 Å. The energy release obtained for this system is −0.54 eV. The binding of H_2S on Au-functionalized Ti_3C_2 occurs with the molecule in a horizontal arrangement: the Au−S bond has a length of 2.74 Å while the separation between H and the closest Au atom is 3.10 Å. An adsorption energy of −0.71 eV is obtained in this case. NH_3 and NO_2 are bound to the surface through Au−N interactions with energy releases of −0.66 and −0.68 eV, respectively. Despite these similar values of adsorption energy, the behavior of the two molecules on the Au-decorated Ti_3C_2 MXene is markedly different. In fact, NH_3 adsorbs at a distance of 2.44 Å between N and Au while NO_2 is much further away from the substrate (N−Au distance: 4.63 Å). We ascribe this behavior to the repulsion exerted to the MXene by the strongly electron-withdrawing NO_2 moiety. Finally, it can be observed that the adsorption of gases is energetically favorable in all cases which is quantified based on negative adsorption energies.

By comparing the adsorption energies obtained for CO, H_2S, and NH_3 on Ti_3C_2 and on its Au-functionalized counterpart, we notice that the computed values are larger for the pristine MXene, see Table 2. This evidence suggests that the gold capping layer screens substrate−adsorbate interactions and it is further supported by their larger separations. We can use the computed values of adsorption energies to assess the performance of the MXene as a sensor for the considered toxic gas molecules, by evaluating the recovery by means of eq 2. The obtained values are listed in Table 2. Among the unreacted gas molecules on pristine Ti_3C_2, CO shows the fastest recovery time of 0.35 μs, making it an ideal analyte for pristine Ti_3C_2-based gas sensors. In contrast, the recovery times calculated for H_2S and NH_3 can be considered infinitely long, indicating that sensing these two gas molecules is not possible on pristine Ti_3C_2. In fact, the substrate cannot return its pristine status in a time window compatible with applications. On the other hand, the recovery times obtained for the toxins at Au−Ti_3C_2 are very reasonable in terms of sensor performance, ranging from 0.21 ns for CO adsorption to about one second for H_2S. Intermediate results are obtained for phosgene (1.60 ms), NH_3 (130 ms), and NO_2 (320 ms). These results indicate that gold functionalization of Ti_3C_2 can improve the detection of gaseous toxins compared to pristine material. Moreover, a comparison of performance parameters for various gas sensors is given in Table 3, indicating the superiority of the studied material over others reported in literature.

3.2. Charge Density Difference Analysis. After the assessment of the adsorption properties of Ti_3C_2 and its Au-functionalized counterparts, it is relevant to analyze the electronic properties of the composite systems. We start by considering the electron density difference between the electron density of the composite system and the one of its constituents. The visualization of this quantity helps understand the charge transfer or redistribution between the interacting systems and collect information about the nature of the chemical interactions in the complex. The charge transfer between pristine Ti_3C_2 and the unreacted gases is

https://doi.org/10.1021/acsomega.4c09428
ACS Omega 2025, 10, 1562−1570

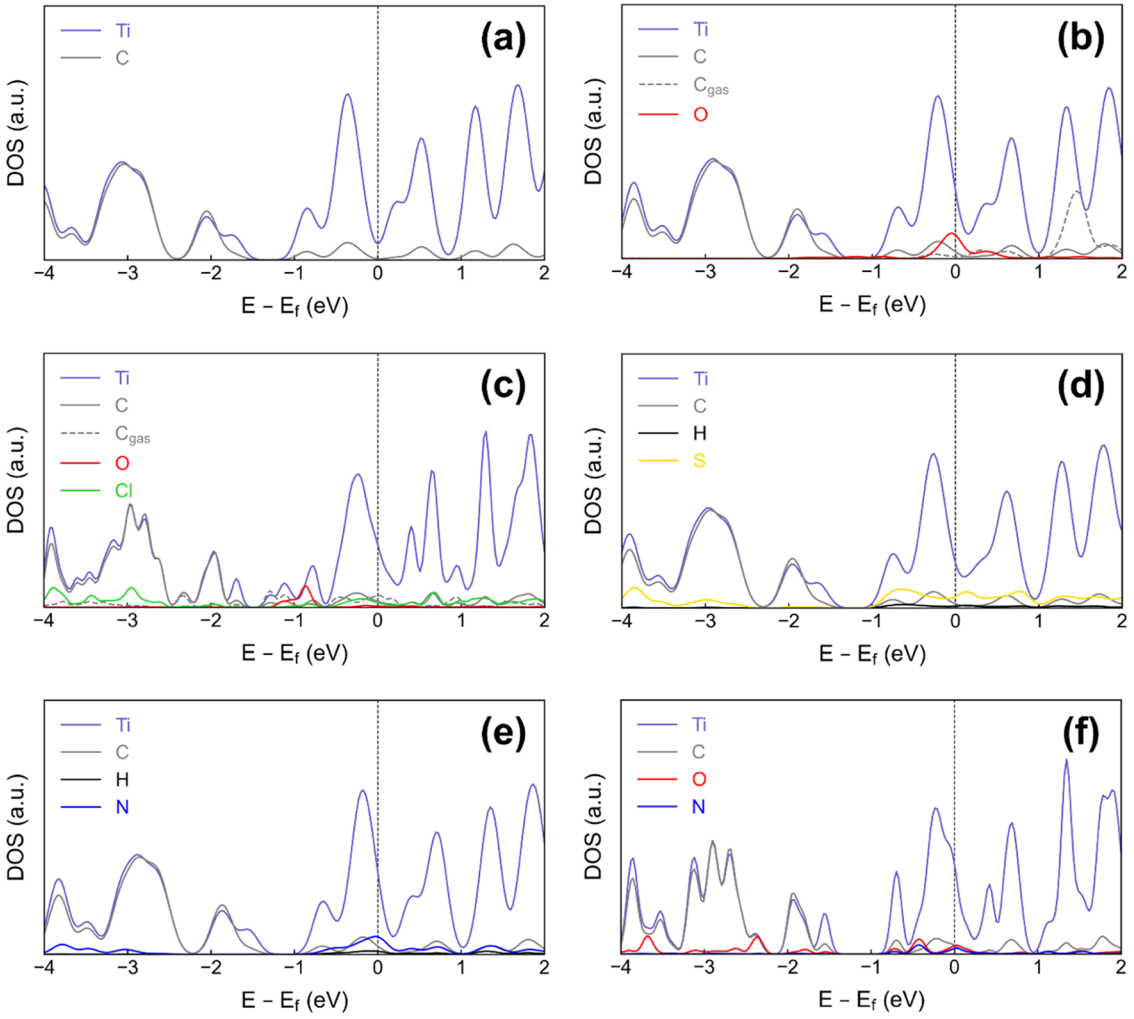

Figure 6. Projected density of states for (a) Ti_3C_2, (b) $CO@Ti_3C_2$, (c) $COCl_2@Ti_3C_2$, (d) $H_2S@Ti_3C_2$, (e) $NH_3@Ti_3C_2$, and (f) $NO_2@Ti_3C_2$. The Fermi energy (E_f) is set at zero.

illustrated in Figure 4. It can be observed that a small amount of electron density is distributed between O and Ti in the $CO@Ti_3C_2$ system confirming the presence of the Ti−O chemical bond. In the $H_2S@Ti_3C_2$ system, a relatively large electron accumulation between S and adjacent Ti atoms is obtained, indicating the formation of a Ti−S chemical bond. Similarly, in the $NH_3@Ti_3C_2$ system, the Ti−N bond can be visualized since electron density is concentrated between N and Ti atoms. Furthermore, it can be noted that in all studied systems, electron density is withdrawn from the Ti atom. The low adsorption energy of $CO@Ti_3C_2$ can be attributed to small charge transfer whereas the large electron density transfer in $H_2S@Ti_3C_2$ and $NH_3@Ti_3C_2$ is responsible for their relatively high binding energies.

The electron density difference isosurfaces for the gas@Au−Ti_3C_2 systems are depicted in Figure 5. It can be noticed that all the investigated toxic gases interact with the Au−Ti_3C_2 surface via weak intermolecular interactions, since in all cases most of the electron density is situated around the atoms and not at the gas-MXene interface. The weak intermolecular forces between gases and Au-decorated MXene can be accountable for comparatively lower binding energies and larger bond distances.

3.3. Density of States and Work Function. Next, we examine the electronic structure of the studied systems with the aid of the projected density of states, see in Figures 6 and 7. The metallic character of Ti_3C_2 is evident in Figure 6a where the populated region crossing the Fermi level is expectedly dominated by Ti-states. Interestingly, the density of states of pristine Ti_3C_2 slightly changes after adsorption. These variations mainly consist of an upshift of the electronic states around the Fermi level (Figure 6b−f). In addition, the electronic population of CO, H_2S, and NH_3 molecules around the Fermi level indicates strong interactions between the sensor and analyte. The smearing of electronic states of the H_2S molecule is likely due to the redistribution of the electron density around adjacent Ti atoms, see Figure 4.

The projected density of states of Au-functionalized Ti_3C_2 MXene [Figure 7(a)] indicates that the MXene remains metallic even in the presence of Au surface modification. The overlap of Au and Ti density of states around the Fermi level shows the Au−Ti chemical bond visualized in the inset, where the redistribution of electron density (yellow isosurface) causes the surface to become positively charged (cyan isosurface). The density of states of Au−Ti_3C_2 remains unchanged on gas adsorption, as shown in Figure 7(b−f). Moreover, in contrast to the gas@Ti_3C_2 systems, a lower and more smeared density of states is obtained which for the gas molecules, testifying the previously discussed absence of strong chemical interactions between the Au-functionalized Ti_3C_2 substrate and the toxins.

https://doi.org/10.1021/acsomega.4c09428
ACS Omega 2025, 10, 1562−1570

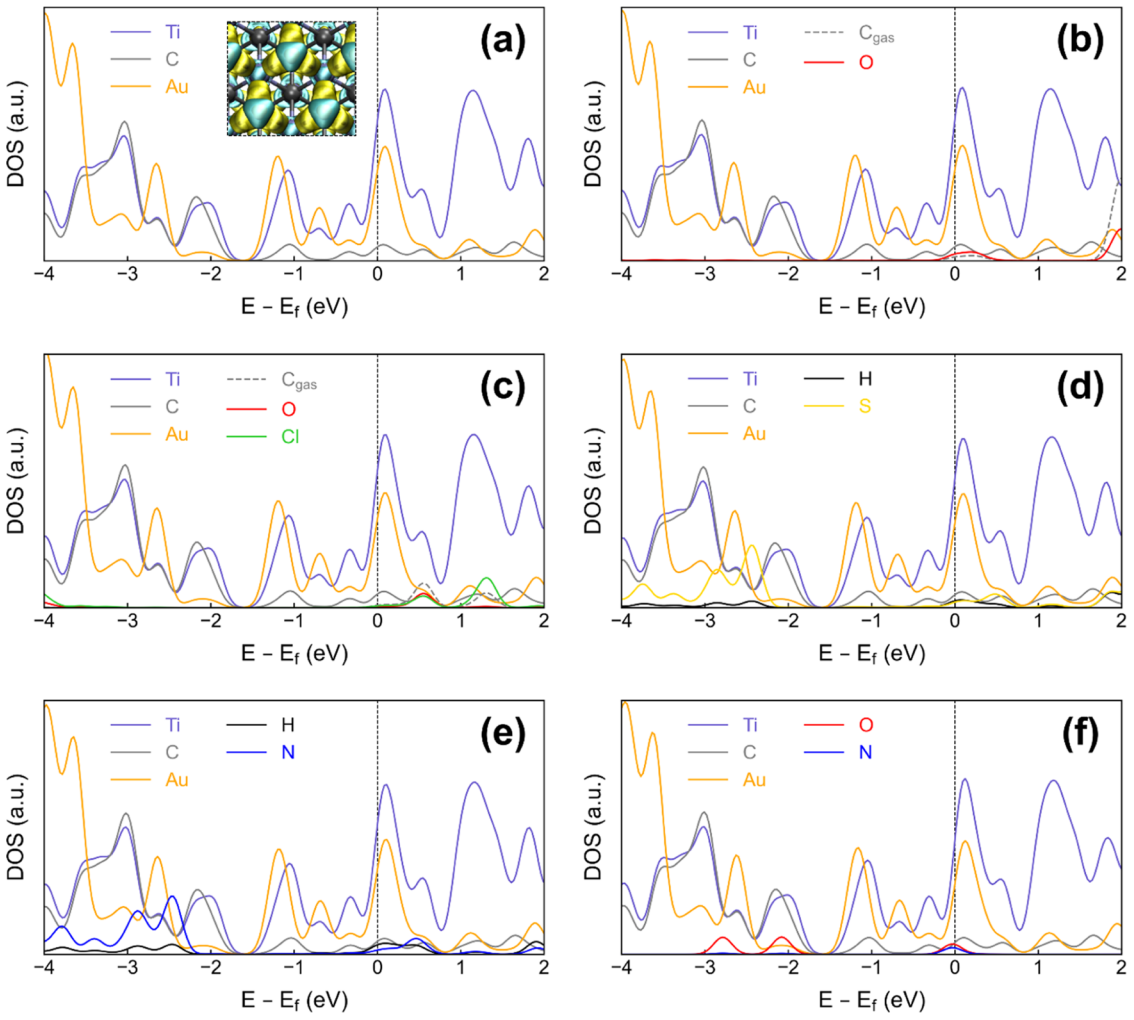

Figure 7. Projected density of states for (a) Au−Ti_3C_2 (inset shows EDD between Au and Ti_3C_2), (b) CO@Au−Ti_3C_2, (c) $COCl_2$@Au−Ti_3C_2, (d) H_2S@Au−Ti_3C_2, (e) NH_3@Au−Ti_3C_2, and (f) NO_2@Au−Ti_3C_2. The Fermi energy (E_f) is set at zero.

Table 4. Estimated Work Function (ϕ), Shift in Work Function ($\Delta\phi$), and Bader Charge (Q) on Gas Molecule for the Studied Systems

system	ϕ (eV)	$\Delta\phi$ (eV)	Q (e^-)
Ti_3C_2	1.82		
CO@Ti_3C_2	1.76	−0.06	0.17
H_2S@Ti_3C_2	1.92	0.10	0.28
NH_3@Ti_3C_2	1.84	0.02	0.02
Au−Ti_3C_2	4.94		
CO@Au−Ti_3C_2	5.01	0.07	0.01
$COCl_2$@Au−Ti_3C_2	5.18	0.24	0.38
H_2S@Au−Ti_3C_2	5.07	0.13	0.11
NH_3@Au−Ti_3C_2	5.08	0.14	0.12
NO_2@Au−Ti_3C_2	4.81	−0.13	0.15

The work functions and Bader charges for the considered systems are calculated to further assess the amount of interfacial charge transfer (Table 4). While pristine Ti_3C_2 is characterized by a work function of 1.82 eV, this value increases by more than 2.5 times in the presence of Au-functionalization. Comparing now the work function for each substrate with and without the gas molecules, we notice similar but not identical trends. Adsorption of H_2S and NH_3 leads to an increase in the work function of the pristine MXene by 100 and 20 meV, respectively. In contrast, interaction with CO lowers the work function by 60 meV. This behavior can be understood considering the larger polarity of the Ti−O bond formed between the MXene and this molecule, which withdraws electron from the substrate. A similar rationale can be used to interpret the results obtained for Au-functionalized Ti_3C_2. With all considered toxins except for NO_2, the work function increases compared to the one of the isolated gold-decorated MXene. The computed values range from 70 meV for CO@Au−Ti_3C_2 to 240 meV for $COCl_2$@Au−Ti_3C_2. In the H_2S@Ti_3C_2 system, a large increase in work function is obtained due to the binding of H_2S with two adjacent Ti atoms. Instead, the work function of NO_2@Au−Ti_3C_2 is 140 meV lower than the one of the isolated substrates.

4. CONCLUSIONS

We investigated Ti_3C_2 MXene (pristine and Au-functionalized) for sensing hazardous gases employing DFT calculations. Our findings revealed that the interaction of pristine Ti_3C_2 MXene with CO, H_2S, and NH_3 yields adsorption energies of −0.33, −1.40, and −1.19 eV, respectively. The resulting recovery time is 0.35 μs for CO while it is significantly large with H_2S and NH_3. The analysis of the electronic properties showed that this material chemically reacts with these sample gases limiting its sensitivity as a

https://doi.org/10.1021/acsomega.4c09428
ACS Omega 2025, 10, 1562−1570

sensor. Au-functionalized Ti_3C_2 MXene, on the other hand, showed lower adsorption energy and reduced recovery time, which are characteristics of efficient and highly sensitive gas sensing materials. Notably, the Au-functionalized Ti_3C_2 MXene displayed exceptional sensing properties for CO with the lowest adsorption energy (−0.14 eV) and the shortest recovery time (0.21 ns) among studied sample gases. For $COCl_2$, H_2S, NH_3, and NO_2, the adsorption energies are −0.54, −0.71, −0.66, and −0.68 eV, respectively, resulting in recovery times ranging from 1.60 ms (with H_2S) to about 1 s (with $COCl_2$). The analysis of the electronic interactions of these composite materials revealed that the metallic nature of the MXene (both pristine and Au-functionalized) is unaltered on gas adsorption. The effect of the physisorbed toxins is to shift by a few hundreds of meV the electronic bands of the substrate, leading to corresponding variations in the calculated work function. This study shows that gold functionalization renders the MXene an effective detector of the sample gaseous toxins. In fact, the noble metal capping layer decreases the binding strength with the adsorbates and thus reduces the recovery time, making it suitable for sensing applications. The results presented in this work provide a basis for further theoretical and experimental investigations on Au-functionalized MXenes as promising materials for effective sensing of hazardous and toxic gases.

AUTHOR INFORMATION

Corresponding Author

Zaheer Ul-Haq − *H.E.J. Research Institute of Chemistry, International Center for Chemical and Biological Sciences, University of Karachi, Karachi 75270, Pakistan;* orcid.org/0000-0002-8530-8711; Email: zaheer.qasmi@iccs.edu

Authors

Muhammad Huzaifa − *H.E.J. Research Institute of Chemistry, International Center for Chemical and Biological Sciences, University of Karachi, Karachi 75270, Pakistan*

Muhammad Shafiq − *H.E.J. Research Institute of Chemistry, International Center for Chemical and Biological Sciences, University of Karachi, Karachi 75270, Pakistan;* orcid.org/0009-0007-8370-9056

Nida Ali − *H.E.J. Research Institute of Chemistry, International Center for Chemical and Biological Sciences, University of Karachi, Karachi 75270, Pakistan*

Caterina Cocchi − *Carl von Ossietzky Universität Oldenburg, Institute of Physics, D-26129 Oldenburg, Germany;* orcid.org/0000-0002-9243-9461

Mohammad Nur-e-Alam − *Department of Pharmacognosy, College of Pharmacy, King Saud University, Riyadh 11451, Kingdom of Saudi Arabia*

Complete contact information is available at: https://pubs.acs.org/10.1021/acsomega.4c09428

Notes

The authors declare no competing financial interest.

ACKNOWLEDGMENTS

The authors extend their appreciation to the Researchers Supporting Project number (RSPD2024R994), King Saud University, Riyadh, Saudi Arabia.

REFERENCES

(1) Stetter, J. R.; Penrose, W. R.; Yao, S. Sensors, chemical sensors, electrochemical sensors, and ECS. *J. Electrochem. Soc.* **2003**, *150* (2), No. S11.

(2) Sun, Y.; Li, Y. Potential environmental applications of MXenes: A critical review. *Chemosphere* **2021**, *271*, No. 129578.

(3) Liu, X.; Ma, T.; Pinna, N.; Zhang, J. Two-dimensional nanostructured materials for gas sensing. *Adv. Funct. Mater.* **2017**, *27* (37), No. 1702168.

(4) Jiménez-Cadena, G.; Riu, J.; Rius, F. X. Gas sensors based on nanostructured materials. *Analyst* **2007**, *132* (11), 1083−1099.

(5) Glavin, N. R.; Rao, R.; Varshney, V.; Bianco, E.; Apte, A.; Roy, A.; Ringe, E.; Ajayan, P. M. Emerging applications of elemental 2D materials. *Adv. Mater.* **2020**, *32* (7), No. 1904302.

(6) Anichini, C.; Czepa, W.; Pakulski, D.; Aliprandi, A.; Ciesielski, A.; Samorì, P. Chemical sensing with 2D materials. *Chem. Soc. Rev.* **2018**, *47* (13), 4860−4908.

(7) Capone, S.; Forleo, A.; Francioso, L.; Rella, R.; Siciliano, P.; Spadavecchia, J.; Presicce, D.; Taurino, A. Solid state gas sensors: state of the art and future activities. *J. Optoelectron. Adv. Mater.* **2003**, *5* (5), 1335−1348.

(8) Babad, H.; Zeiler, A. G. Chemistry of phosgene. *Chem. Rev.* **1973**, *73* (1), 75−91.

(9) Raub, J. A.; Mathieu-Nolf, M.; Hampson, N. B.; Thom, S. R. Carbon monoxide poisoning—a public health perspective. *Toxicology* **2000**, *145* (1), 1−14.

(10) Holloway, T.; Levy, H.; Kasibhatla, P. Global distribution of carbon monoxide. *J. Geophys. Res.: Atmos.* **2000**, *105* (D10), 12123−12147.

(11) Motterlini, R.; Otterbein, L. E. The therapeutic potential of carbon monoxide. *Nat. Rev. Drug Discovery* **2010**, *9* (9), 728−743.

(12) Tikuisis, P.; Kane, D.; McLellan, T.; Buick, F.; Fairburn, S. Rate of formation of carboxyhemoglobin in exercising humans exposed to carbon monoxide. *J. Appl. Physiol.* **1992**, *72* (4), 1311−1319.

(13) Ernst, A.; Zibrak, J. D. Carbon monoxide poisoning. *N. Engl. J. Med.* **1998**, *339* (22), 1603−1608.

(14) Wegener, G.; Brandt, M.; Duda, L.; Hofmann, J.; Klesczewski, B.; Koch, D.; Kumpf, R.-J.; Orzesek, H.; Pirkl, H.-G.; Six, C.; et al. Trends in industrial catalysis in the polyurethane industry. *Appl. Catal., A* **2001**, *221* (1−2), 303−335.

(15) Liu, A.-H.; Li, Y.-N.; He, L.-N. Organic synthesis using carbon dioxide as phosgene-free carbonyl reagent. *Pure Appl. Chem.* **2011**, *84* (3), 581−602.

(16) Cucinell, S. A.; Arsenal, E. Review of the toxicity of long-term phosgene exposure. *Arch. Environ. Health: Int. J.* **1974**, *28* (5), 272−275.

(17) Quadrelli, E. A.; Centi, G.; Duplan, J. L.; Perathoner, S. Carbon dioxide recycling: emerging large-scale technologies with industrial potential. *ChemSusChem* **2011**, *4* (9), 1194−1215.

(18) Deji, R.; Nagy, G.; Choudhary, B.; Sharma, R. K.; Kashyap, M. K.; Kahaly, M. U. Atomic ordered doping leads to enhanced sensitivity of phosgene gas detection in graphene nanoribbon: a quantum DFT approach. *Phys. Scr.* **2024**, *99* (3), No. 035931.

(19) Deji, R.; Verma, A.; Kaur, N.; Choudhary, B.; Sharma, R. K. Density functional theory study of carbon monoxide adsorption on transition metal doped armchair graphene nanoribbon. *Mater. Today: Proc.* **2022**, *54*, 771−776.

(20) Ebadi, M.; Reisi-Vanani, A. Methanol and carbon monoxide sensing and capturing by pristine and Ca-decorated graphdiyne: A DFT-D2 study. *Phys. E* **2021**, *125*, No. 114425.

(21) Ghambarian, M.; Azizi, Z.; Ghashghaee, M. Remarkable improvement in phosgene detection with a defect-engineered phosphorene sensor: first-principles calculations. *Phys. Chem. Chem. Phys.* **2020**, *22* (17), 9677−9684.

(22) Ghambarian, M.; Azizi, Z.; Ghashghaee, M. Phosphorene defects for high-quality detection of nitric oxide and carbon monoxide: A periodic density functional study. *Chem. Eng. J.* **2020**, *396*, No. 125247.

(23) Chen, Z.; Li, R.; Peng, X.; Jiang, H.; Zeng, H. Exploring adsorption and sensing mechanism of Li-decorated N-doped black phosphorene for toxic gases: Insights from first-principles calculations. *Surf. Interfaces* **2024**, *52*, No. 104872.
(24) Sharma, A.; Khan, M. S.; Husain, M. Adsorption of phosgene on Si-embedded MoS 2 sheet and electric field-assisted desorption: insights from DFT calculations. *J. Mater. Sci.* **2019**, *54*, 11497−11508.
(25) Liu, Y.; Yang, Z.; Huang, L.; Zeng, W.; Zhou, Q. Anti-interference detection of mixed NOX via In2O3-based sensor array combining with neural network model at room temperature. *J. Hazard. Mater.* **2024**, *463*, No. 132857.
(26) Zhang, Y.; Feng, W.; Hou, W.; Zeng, W.; Zhou, Q. Experimental and density functional theory study of the gas sensing property of Pt and Au doped WS2 to partial discharge gas CO in air switchgear. *Sens. Actuators, A* **2024**, *379*, No. 115905.
(27) Lu, D.; Huang, L.; Zhang, J.; Zeng, W.; Zhou, Q. Pt decorated Janus WSSe monolayer: A gas-sensitive material candidate for SF6 decomposition gases based on the first-principles. *J. Environ. Chem. Eng.* **2024**, *12* (2), No. 112388.
(28) Gogotsi, Y.; Anasori, B. *The Rise of MXenes*; ACS Publications, 2019; Vol. *13*, pp 8491−8494.
(29) Lee, E.; Kim, D.-J. Recent exploration of two-dimensional MXenes for gas sensing: From a theoretical to an experimental view. *J. Electrochem. Soc.* **2020**, *167* (3), No. 037515.
(30) Bhargava Reddy, M. S.; Kailasa, S.; Marupalli, B. C.; Sadasivuni, K. K.; Aich, S. A family of 2D-MXenes: synthesis, properties, and gas sensing applications. *ACS Sens.* **2022**, *7* (8), 2132−2163.
(31) Liu, X.; Zhang, H.; Song, Y.; Shen, T.; Sun, J. Facile solvothermal synthesis of ZnO/Ti3C2Tx MXene nanocomposites for NO2 detection at low working temperature. *Sens. Actuators, B* **2022**, *367*, No. 132025.
(32) Wu, M.; He, M.; Hu, Q.; Wu, Q.; Sun, G.; Xie, L.; Zhang, Z.; Zhu, Z.; Zhou, A. Ti3C2MXene-based sensors with high selectivity for NH3 detection at room temperature. *ACS Sens.* **2019**, *4* (10), 2763−2770.
(33) Boonpalit, K.; Kinchagawat, J.; Prommin, C.; Nutanong, S.; Namuangruk, S. Efficient exploration of transition-metal decorated MXene for carbon monoxide sensing using integrated active learning and density functional theory. *Phys. Chem. Chem. Phys.* **2023**, *25* (42), 28657−28668.
(34) Zheng, Z.; Feng, X.; Feng, L.; Feng, X. Adsorption sensitivity and sensing performance of Au-doped Ti3C2O2 gas sensor for fault characteristic gases in power transformer. *Mol. Phys.* **2024**, No. e2368723.
(35) Panigrahi, P.; Pal, Y.; Kaewmaraya, T.; Bae, H.; Nasiri, N.; Hussain, T. Molybdenum carbide MXenes as efficient nanosensors toward selected chemical warfare agents. *ACS Appl. Nano Mater.* **2023**, *6* (10), 8404−8415.
(36) Xu, Q.; Zong, B.; Li, Q.; Fang, X.; Mao, S.; Ostrikov, K. K. H2S sensing under various humidity conditions with Ag nanoparticle functionalized Ti3C2Tx MXene field-effect transistors. *J. Hazard. Mater.* **2022**, *424*, No. 127492.
(37) Mostafaei, A.; Abbasnejad, M. Computational studies on the structural, electronic and optical properties of M2CT2 (M= Y, Sc and T= F, Cl) MXene monolayer. *J. Alloys Compd.* **2021**, *857*, No. 157982.
(38) Naguib, M.; Kurtoglu, M.; Presser, V.; Lu, J.; Niu, J.; Heon, M.; Hultman, L.; Gogotsi, Y.; Barsoum, M. W. Two-Dimensional Nanocrystals Produced by Exfoliation of Ti3AlC2. In *MXenes*; Jenny Stanford Publishing, 2011; pp 15−29.
(39) Li, L.; Cao, H.; Liang, Z.; Cheng, Y.; Yin, T.; Liu, Z.; Yan, S.; Jia, S.; Li, L.; Wang, J.; Gao, Y. First-principles study of Ti-deficient Ti3C2MXene nanosheets as NH3 gas sensors. *ACS Appl. Nano Mater.* **2022**, *5* (2), 2470−2475.
(40) Hu, C.; Yu, X.; Li, Y.; Cheng, J.; Li, Q.; Xiao, B. Bandgap engineering of strained S-terminated MXene and its promising application as NOx gas sensor. *Appl. Surf. Sci.* **2022**, *592*, No. 153296.
(41) Naqvi, S. R.; Shukla, V.; Jena, N. K.; Luo, W.; Ahuja, R. Exploring two-dimensional M2NS2 (M= Ti, V) MXenes based gas sensors for air pollutants. *Appl. Mater. Today* **2020**, *19*, No. 100574.
(42) K Choudhury, R.; Bhagat, B.; Mali, K.; Pokar, R.; Dashora, A. Effect of surface functional group over tungsten carbide MXene for efficient NH3 gas sensing using density functional theory. *Appl. Surf. Sci.* **2022**, *603*, No. 154426.
(43) Junkaew, A.; Arroyave, R. Enhancement of the selectivity of MXenes (M 2 C, M= Ti, V, Nb, Mo) via oxygen-functionalization: promising materials for gas-sensing and-separation. *Phys. Chem. Chem. Phys.* **2018**, *20* (9), 6073−6082.
(44) Khakbaz, P.; Moshayedi, M.; Hajian, S.; Soleimani, M.; Narakathu, B. B.; Bazuin, B. J.; Pourfath, M.; Atashbar, M. Z. Titanium carbide MXene as NH3 sensor: realistic first-principles study. *J. Phys. Chem. C* **2019**, *123* (49), 29794−29803.
(45) Shuvo, S. N.; Ulloa Gomez, A. M.; Mishra, A.; Chen, W. Y.; Dongare, A. M.; Stanciu, L. A. Sulfur-doped titanium carbide MXenes for room-temperature gas sensing. *ACS Sens.* **2020**, *5* (9), 2915−2924.
(46) Chen, W. Y.; Sullivan, C. D.; Lai, S.-N.; Yen, C.-C.; Jiang, X.; Peroulis, D.; Stanciu, L. A. Noble-Nanoparticle-Decorated Ti3C2T x MXenes for Highly Sensitive Volatile Organic Compound Detection. *ACS Omega* **2022**, *7* (33), 29195−29203.
(47) Kühne, T. D.; Iannuzzi, M.; Del Ben, M.; Rybkin, V. V.; Seewald, P.; Stein, F.; Laino, T.; Khaliullin, R. Z.; Schütt, O.; Schiffmann, F.; et al. CP2K: An electronic structure and molecular dynamics software package-Quickstep: Efficient and accurate electronic structure calculations. *J. Chem. Phys.* **2020**, *152* (19), No. 194103, DOI: 10.1063/5.0007045.
(48) VandeVondele, J.; Hutter, J. Gaussian basis sets for accurate calculations on molecular systems in gas and condensed phases. *J. Chem. Phys.* **2007**, *127* (11), No. 114105, DOI: 10.1063/1.2770708.
(49) Goedecker, S.; Teter, M.; Hutter, J. Separable dual-space Gaussian pseudopotentials. *Phys. Rev. B* **1996**, *54* (3), No. 1703.
(50) Perdew, J. P.; Burke, K.; Ernzerhof, M. Generalized gradient approximation made simple. *Phys. Rev. Lett.* **1996**, *77* (18), No. 3865.
(51) Grimme, S.; Antony, J.; Ehrlich, S.; Krieg, H. A consistent and accurate ab initio parametrization of density functional dispersion correction (DFT-D) for the 94 elements H-Pu. *J. Chem. Phys.* **2010**, *132* (15), No. 154104, DOI: 10.1063/1.3382344.
(52) Otero-de-la-Roza, A.; Johnson, E. R.; Luaña, V. Critic2: A program for real-space analysis of quantum chemical interactions in solids. *Comput. Phys. Commun.* **2014**, *185* (3), 1007−1018.
(53) Humphrey, W.; Dalke, A.; Schulten, K. VMD: visual molecular dynamics. *J. Mol. Graphics* **1996**, *14* (1), 33−38.
(54) Zhang, J.-N.; Ma, L.; Zhang, M.; Zhang, J.-M. Effects of gas adsorption on electronic and optical properties of palladium-doped graphene: First-principles study. *Phys. E* **2020**, *118*, No. 113879.
(55) Patel, K.; Roondhe, B.; Dabhi, S. D.; Jha, P. K. A new flatland buddy as toxic gas scavenger: A first principles study. *J. Hazard. Mater.* **2018**, *351*, 337−345.
(56) Peng, S.; Cho, K.; Qi, P.; Dai, H. Ab initio study of CNT NO2 gas sensor. *Chem. Phys. Lett.* **2004**, *387* (4−6), 271−276.
(57) Lang, N. D.; Kohn, W. Theory of metal surfaces: work function. *Phys. Rev. B* **1971**, *3* (4), No. 1215.
(58) Liu, Y.; Li, J.; Hou, W.; Zhou, Q.; Zeng, W. Pristine and Ag decorated In2O3 (110): A gas-sensitive material to selective detect NO2 based on DFT study. *J. Mater. Res. Technol.* **2022**, *18*, 4236−4247.
(59) Zhao, Y.; Wu, Y.; Lu, S. Unexpected Bi-functional Co-g-GaN monolayer for detecting and scavenging toxic gases. *Mater. Today Commun.* **2023**, *35*, No. 105781.
(60) Xiong, H.; Liu, B.; Zhang, H.; Qin, J. Theoretical insight into two-dimensional M-Pc monolayer as an excellent material for formaldehyde and phosgene sensing. *Appl. Surf. Sci.* **2021**, *543*, No. 148805.
(61) Ghadiri, M.; Ghashghaee, M.; Ghambarian, M. Mn-Doped black phosphorene for ultrasensitive hydrogen sulfide detection: periodic DFT calculations. *Phys. Chem. Chem. Phys.* **2020**, *22* (27), 15549−15558.

https://doi.org/10.1021/acsomega.4c09428
ACS Omega 2025, 10, 1562−1570

(62) Lu, D.; Huang, L.; Zhang, J.; Zhang, Y.; Feng, W.; Zeng, W.; Zhou, Q. Rh-and Ru-modified InSe monolayers for detection of NH3, NO2, and SO2 in agricultural greenhouse: a DFT study. *ACS Appl. Nano Mater.* **2023**, *6* (15), 14447−14458.

https://doi.org/10.1021/acsomega.4c09428
ACS Omega 2025, 10, 1562−1570